Van Beek, V. M. *et al.* (2015). *Géotechnique* **65**, No. 9, 740–754 [http://dx.doi.org/10.1680/geot.14.P.119]

Developments in modelling of backward erosion piping

V. M. VAN BEEK*, H. M. VAN ESSEN†, K. VANDENBOER‡ and A. BEZUIJEN§

One of the failure mechanisms that can affect the safety of a dyke or another water-retaining structure is backward erosion piping, a phenomenon that results in the formation of shallow pipes at the interface of a sandy or silty foundation and a cohesive cover layer. The models available for predicting the critical head at which the pipe progresses to the upstream side have been validated and adapted on the basis of experiments with two-dimensional (2D) configurations. However, the experimental base for backward erosion in three-dimensional (3D) configurations in which the flow concentrates towards one point, a situation that is commonly encountered in the field, is limited. This paper presents additional 3D configuration experiments at two scales with a range of sand types. The critical gradients, the formed pipes and the erosion mechanism were analysed for the available experiments, indicating that the erosion mechanism is more complex than previously assumed, as both erosion at the tip of the pipe (primary erosion) and in the pipe (secondary erosion) are relevant. In addition, a 3D configuration was found to result in significantly lower critical gradients than those predicted by an accepted calculation model calibrated on the basis of 2D experiments, a finding that is essential for the application of the model in the field.

KEYWORDS: design; embankments; erosion

INTRODUCTION

Backward erosion piping is an internal erosion mechanism that can result in a loss of stability in water-retaining structures. This paper focuses specifically on the type of backward erosion piping that occurs in the granular foundation of dams and dykes consisting of uniform silts and sands, and covered by a cohesive layer. The head loss across the structure results in a flow through the aquifer, and the convergence of flow lines near the downstream exit causes the sand bed to fluidise locally (Van Beek *et al.*, 2014a). Subsequent erosion leads to the development of shallow pipes at the interface of the aquifer and the cohesive top layer. After the full development of the pipe to the upstream water level, the increased flow causes the deepening and widening of the pipe, undermining the structure.

The specific conditions described are often met on rivers, where sand boils have been observed downstream of the dykes when water levels are high (see, e.g. Mansur *et al.*, 2000; Vrijling *et al.*, 2010). Sand boils often occur at locations where the flow concentrates towards the surface (USACE, 1956). Several dyke failures have been attributed to backward erosion piping, examples being the failures near Zalk, Nieuwkuijk and Tholen in the Netherlands early last century (Vrijling *et al.*, 2010), one of the failures in the levee system of New Orleans as a result of Katrina (Vrijling *et al.*, 2010), and several cases in China on the Yangtze and Nenjiang rivers as a result of the 1998 flood (Yao *et al.*, 2009).

The earliest design and prediction models date back to early last century (Bligh, 1910; Lane, 1935) and, despite the criticisms levelled at them, they are still used. On the basis of data derived from specific cases of piping, empirical relationships were established to determine the critical head (H_c), which is defined as the head across the structure at which the piping process results in ongoing erosion, finally leading to failure. These empirical rules linked the critical head to the seepage length L and the soil properties. The seepage length is defined here as the distance that the pipe must cover between the upstream level and downstream level, as illustrated in Fig. 1.

More recent attempts to describe the process look at either pipe initiation or pipe progression. Pipe initiation, which is marked by the transition from an intact sand bed to a sand bed with a short pipe caused by the initiation of sand transport, can be described by the flow conditions in the sand bed near the exit, and it has been investigated in Richards & Reddy (2012) and Van Beek *et al.* (2014a). Once the pipe has initiated, equilibrium can be observed in pipe formation, requiring the increase in head difference H to make the pipe progress. Modelling the progression of the pipe therefore requires combining the analysis of pipe flow, groundwater flow and criteria for erosion in and around the pipe.

Several attempts have been made to describe or model these processes in whole or in part. Hanses (1985), Sellmeijer (1988), Sellmeijer *et al.* (2011) and Schmertmann (2000) have published models, which are briefly described by Van Beek *et al.* (2014a). Hanses (1985) assumed that 'primary erosion' – erosion at the tip of the pipe – causes pipe lengthening. He simulated the flow pattern in the experiments and included the impact of the pipe on groundwater flow using the pipe gradients measured during the experiments. The Sellmeijer model is the only backward erosion model that explicitly includes the pipe hydraulics and the equilibrium of forces on the particles at the bottom of the pipe just before erosion starts (Sellmeijer, 1988). In this two-dimensional (2D) model, secondary erosion – defined as erosion that results in the widening or deepening of the pipe – is assumed to be the main mechanism of pipe development. Recently, the model was adapted to account for the influence of soil characteristics in the light of experimental results (Sellmeijer *et al.*, 2011), making it more empirical in nature. The lack of a proper explanation for this entirely empirical adaptation is unsatisfactory and limits its practical use to sand types similar to

Manuscript received 29 June 2014; revised manuscript accepted 23 April 2015. Published online ahead of print 22 July 2015.
Discussion on this paper closes on 1 February 2016, for further details see p. ii.
* Unit Geo-Engineering, Deltares, Delft, the Netherlands; Faculty of Civil Engineering and Geosciences, Delft University of Technology, Delft, the Netherlands.
† Unit Geo-Engineering, Deltares, Delft, the Netherlands.
‡ Department Civil Engineering, Ghent University, Ghent, Belgium.
§ Department Civil Engineering, Ghent University, Ghent, Belgium; Unit Geo-Engineering, Deltares, Delft, the Netherlands.

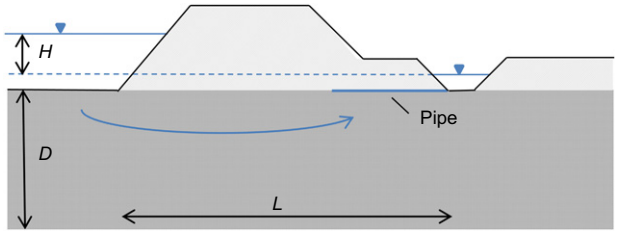

Fig. 1. Schematised dyke with sandy or silty foundation

those investigated. Schmertmann (2000) developed a model, the point method, which relies mainly on the observed variations of critical gradients in experiments. It uses the concept that the local seepage gradient below the pipe determines its advance. Flow nets (without pipe) are used to link the local gradient required for pipe progression in experiments to the local gradient along the pipe path in a field situation. This approach disregards the impact of the pipe on the groundwater flow. Neither model considers grain transport.

In the past, all available piping experiments have been used for the validation and calibration of the prediction models. Recent research (Van Beek *et al.*, 2014a) shows that this is incorrect. Only experiments in which the critical head is dominated by the process of progression should be used for the validation of models in which pipe equilibrium is assumed.

Equilibrium in pipe development has been observed in experiments at a large scale (Silvis, 1991; Van Beek *et al.*, 2011) and experiments with a small exit area (Miesel (1978), Müller-Kirchenbauer (1978), Hanses (1985) and some of the experiments by Townsend *et al.*, (1988) and Pietrus (1981)). In these experiments, a pipe is formed that comes to a halt in time in such a way that the head needs to be increased for the pipe to develop further. The hydraulic conditions in and around the pipe therefore determine its progress and the progression head. As in all of the piping experiments analysed in this paper, the head required for pipe progression (H_p) is the same as the critical head (H_c) and it will therefore be referred to as such in the rest of this paper.

Although several experimental series are available in which pipe progression determines the critical head, the influence of soil type on the critical head has, until now, been mainly studied in experiments without equilibrium. In addition, most experiments until now have been performed in a 2D geometry, whereas sand boils tend to occur in areas where the flow concentrates towards the exit in a three-dimensional (3D) geometry (USACE, 1956).

This paper describes a set of experiments in which the influences of soil characteristics and scale on critical head were investigated using a 3D configuration. The 3D configuration, consisting of a box with a circular exit hole, ensured pipe initiation at a relatively low head so that equilibrium was likely to occur during the experiment. The critical heads obtained were compared with predictions using the Sellmeijer model. However, although useful for examining trends, a comparison of critical heads does not explain why differences are found between experiment and model calculations. For a better understanding of the process involved, additional analyses with respect to the pipe width and depth, its impact on the flow pattern and the erosion mechanism were conducted. The findings were combined in a discussion of the erosion mechanism.

THREE-DIMENSIONAL EXPERIMENTS AVAILABLE IN THE LITERATURE

In all available experiments, a sand bed covered by an impermeable layer has been subjected to a hydraulic gradient. The main differences relate to the type of inlet and outlet, the scale and the sand type. The experiments in which the progression of the pipe dominated the critical head are the relatively large-scale experiments or those with a small exit area. In these experiments it has been found that pipe formation stops after some time so that an increase in head was necessary for pipe development to continue.

Silvis (1991) and Van Beek *et al.* (2011) described the available large-scale experiments, which are known to be well predicted by the Sellmeijer model (Weijers & Sellmeijer, 1993; Sellmeijer *et al.*, 2011). The experiments in both of these studies were performed with a 2D configuration, although the type of outlet was different: in the experiments by Silvis, the water exits towards a ditch, whereas in the experiments by Van Beek *et al.* (2011), the water exits to a large area.

Experiments with a small exit area were conducted by Townsend *et al.* (1988) and Pietrus (1981), also by Hanses (1985) and Miesel (1978). It should be noted that only experiments in single sand layers are considered in this paper.

In the experiments by Townsend *et al.* (1988) and Pietrus (1981), an artificial pipe was created before starting the experiment. These experiments are therefore not suitable for progression analysis since the pipe dimensions do not match the natural pipe dimensions.

The experiments by Hanses (1985) and Miesel (1978) were performed in a 3D set-up, with water exiting to a circular hole in the cover layer. Both Hanses and Miesel simulated the presence of a thick soft soil layer by extending the exit point to the simulated surface using a vertical tube. The head loss originating from this vertical section was measured in the experiments by Hanses (1985), allowing for the head at which the pipe progressed to be corrected for this head loss.

Miesel (1978) investigated the effect of exit hole diameter on the process and the critical head. The critical head was found to increase slightly with the increase in the exit hole diameter (an increase of approximately 15 to 19 cm associated with an increase in the size of the exit hole from 2·5 to 13 cm). As the exit loss (the head loss resulting from flow through the vertical section of the exit hole) is not known for these experiments, the critical heads obtained by Miesel will not be analysed in more detail here.

Hanses (1985) investigated the critical head and pipe hydraulics in both single- and multi-layer configurations at different scales. All experiments were performed on sand A, the properties of which are described in Table 1. Table 2 provides an overview of the characteristics of the successful experiments with single sand layers by Hanses (1985). Three of these experiments (26a, 53, 73) were performed specifically to determine the hydraulic gradient in the pipe. Accordingly, in the first phase of the experiment, the hydraulic head was raised until the critical pipe length was reached; in the second phase the hydraulic head was brought back to 0 and reapplied in steps to assess the head loss in the pipe.

EXPERIMENTAL WORK

The experimental work by Hanses (1985) provides valuable information about the effect of set-up dimensions on the critical head. Experimental work looking at the influence of sand characteristics on critical head and pipe hydraulics is

Table 1. Sand characteristics in experiments by Hanses (1985)

Sand type	d_{50}: mm	d_{70}: mm	d_{60}/d_{10}	Min. wet porosity	Max. wet porosity
Sand A	0·325*	0·355*	1·30	0·410	0·510

*Values obtained by extrapolation of d_{10} and d_{60}.

Table 2. Overview of experiments by Hanses (1985)

Exp. no.	Sand type	K: m/s	RD	W: m	L: m	D: m	$Ø$: mm	H_c: m*	H_c/L
21	Sand A	$4{\cdot}0\times10^{-4}$	0·996	0·240	0·720	0·240	6	0·126	0·175
22	Sand A	$4{\cdot}0\times10^{-4}$	1·000	0·240	0·720	0·240	6	0·128	0·178
23	Sand A	$3{\cdot}9\times10^{-4}$	1·017	0·240	0·720	0·240	6	0·127	0·176
24	Sand A	$3{\cdot}7\times10^{-4}$	1·047	0·240	0·720	0·240	6	0·127	0·176
25	Sand A	$4{\cdot}0\times10^{-4}$	0·996	0·240	0·720	0·240	6	0·126	0·175
26a	Sand A	$4{\cdot}2\times10^{-4}$	0·961	0·240	0·720	0·240	6	0·107	0·149
51	Sand A	$4{\cdot}0\times10^{-4}$	0·990	0·165	0·660	0·083	6	0·206	0·312
52	Sand A	$4{\cdot}7\times10^{-4}$	0·868	0·165	0·660	0·083	6	0·200	0·303
53	Sand A	$4{\cdot}4\times10^{-4}$	0·918	0·165	0·660	0·083	6	0·170	0·258
71	Sand A	$4{\cdot}7\times10^{-4}$	0·868	0·660	2·640	0·330	6	0·276	0·105
73	Sand A	$5{\cdot}1\times10^{-4}$	0·800	0·660	2·640	0·330	6	0·275	0·104

*Critical head corrected for exit loss

limited. Additional experiments were therefore conducted to investigate the influence of sand type on the role of critical head in pipe progression. Several experiments have also allowed for the investigation of pipe dimensions, pipe hydraulics and the erosion mechanism.

Experimental set-up

The experiments with an exit hole simulated the case where a confining upper layer is locally punctured such that flow from the aquifer concentrates towards one point. Three types of experiments were performed. They can be described as small-scale experiments, medium-scale experiments and visualisation experiments. In these experiments, a confined sand sample was subjected to a head drop, simulating the flow of water through an aquifer beneath an impermeable water-retaining structure. All experiments were performed using a small circular exit in the top of the box. The high flow velocity near the exit ensured pipe initiation at a relatively low head drop, allowing the process of pipe progression to be investigated.

The dimensions (length, width, height) of the contained sample in the small- and medium-scale experiments were $0{\cdot}48\times0{\cdot}30\times0{\cdot}105$ m and $1{\cdot}913\times0{\cdot}881\times0{\cdot}403$ m, respectively, with seepage lengths of 0·343 m and 1·385 m. On the upstream side, the sand sample was contained by a filter. The top plate in the experiments was transparent and coated with silicone gel on the inside to obtain a relatively rough surface that resembled a clay cover. A circular exit hole was created in the cover for the exit of water flow. A cylinder was submerged in the plate, connected to the outlet and allowance was made for the deposition of sand around the hole (Fig. 2). The visualisation experiment developed to observe the pipe path in cross-section was similar to half of a small-scale experiment; that is, as it were, cut in half along its centre axis such that the exit hole is found on the wall of the box. The dimensions of the box were $0{\cdot}48\times0{\cdot}15\times0{\cdot}10$ m and the seepage length was 0·343 m. To observe the pipe path in cross-section, the side walls were transparent in this set-up.

In most of the small-scale experiments, the exit hole was 6 mm in diameter and it had a height (representing the thickness of the confining layer) of 10 mm. In the medium-scale experiments, in which the dimensions were approximately four times larger in all directions, the exit hole was 20·5 mm and the vertical length was 20 mm. The exit hole was scaled to achieve similar exit flow velocities. In the visualisation experiment, the exit hole was a semicircle with a diameter of 6 mm. In all experiments, the height of the exit hole was small by comparison with the dimensions of the box (10 and 20 mm in the small- and medium-scale experiments) in order to keep exit head losses as low as possible. This contrasted with the height of the exit in the experiments by Hanses (1985), which approximately matched the sand sample depth and resulted in considerable exit losses in some experiments.

In all experiments, the potential was measured using riser tubes or pore pressure transducers placed at various locations in the sand sample box (denoted by h and p, respectively, in Fig. 2). The potential measurements allowed for the calculation of the initial permeability of the intact sand sample (values given later in Table 4) and upstream filter resistance. In the visualisation and medium-scale experiments, riser tubes and pore pressure meters were installed in the cover to analyse the pipe hydraulics.

The sand sample was prepared with the box in an upright position (inlet facing down). Dense samples (relative density $>85\%$) were prepared by sprinkling dry sand into de-aired water during continuous tamping. Loose to medium-dense samples were prepared by sprinkling dry sand into de-aired water so that a loose sample was obtained that was compacted to the required density by applying a pulse. In one of the medium-scale experiments, this method did not result in an entirely homogeneous sample: layering due to segregation during sample preparation was observed, and this had a significant impact on pipe formation. In the second experiment on this type of sand, more continuous tamping and sand sprinkling prevented layering.

The tests were performed by the stepwise increase of a hydraulic head until erosion took place. When sand transport was observed, the increase in the head drop was delayed until the erosion process stabilised, which meant that no sand was transported in or near the pipes and that the flow and heads observed in the riser tubes were constant. In the visualisation experiment, the head drop was brought back to zero at two pipe lengths (175 mm and 230 mm), and reapplied stepwise until erosion continued.

Various sand types were tested. Table 3 gives an overview of the characteristics of these sands. All sands were sieved to remove the fine fraction. Two mixtures were created by adding fines to a sieved fraction. In the small-scale experiments, the relative density and exit hole diameter were also varied. It should be noted that the Itterbeck 330 μm sand applied in the medium-scale experiments was comparable to the Enschede and Hoherstall Waalre sands applied in the small-scale experiments. Different sand types were selected because the last two sand types were not available in large quantities. Table 4 contains an overview of the experiments. In total, three medium-scale experiments, 19 small-scale experiments and one successful visualisation experiment were performed. The resulting critical heads, which are given in Table 4, show that the reproducibility of the small-scale experiments was particularly good in the case of the

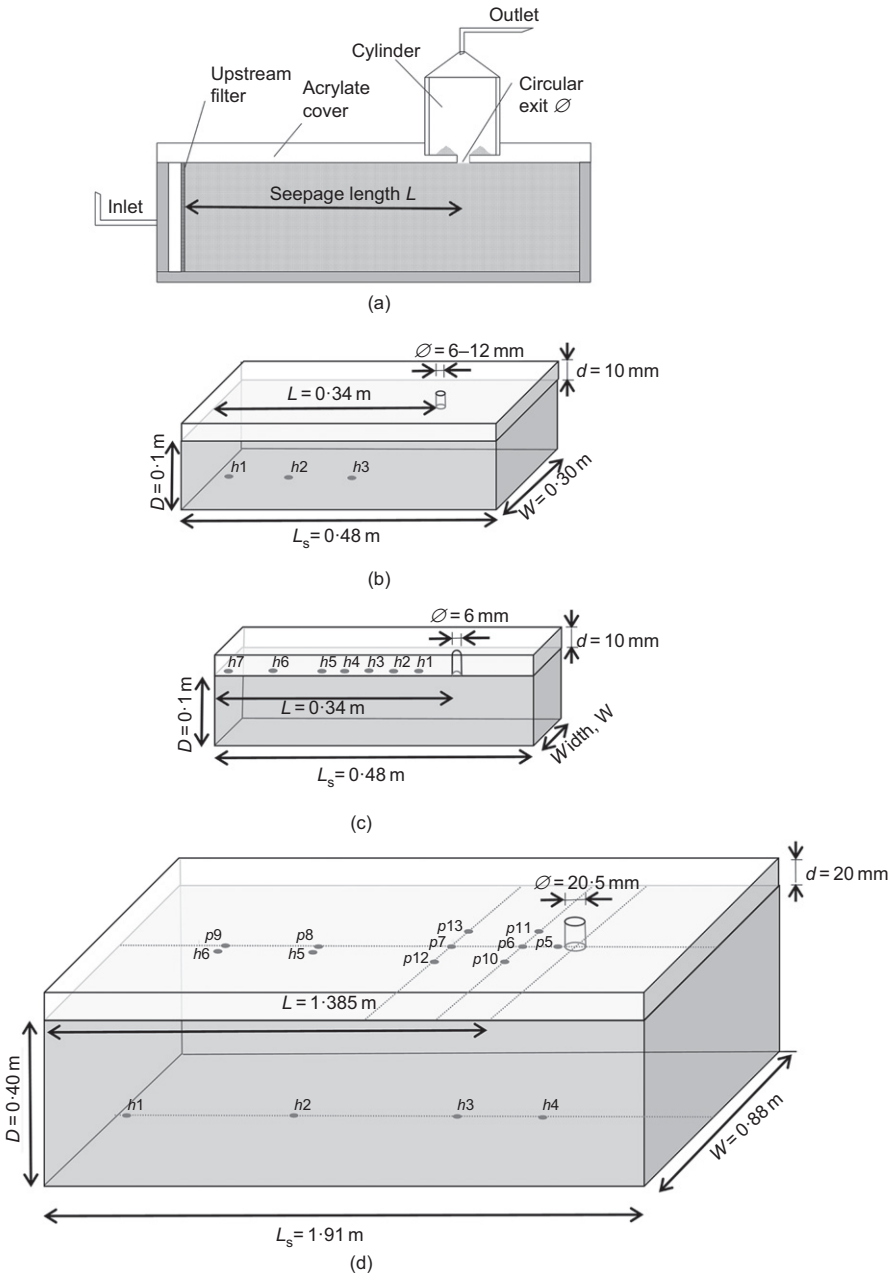

Fig. 2. (a) Schematic diagram of the general experimental set-up; the specific configurations for the (b) small-scale, (c) visualisation and (d) medium-scale experiments, showing the set-up dimensions and locations of the riser tubes and pore pressure transducers

Table 3. Sand characteristics in additional experiments

Sand type	d_{50}: mm	d_{70}: mm	d_{60}/d_{10}	Min. wet porosity*	Max. wet porosity*
Baskarp 1	0·132	0·154	1·54	0·340	0·469
Baskarp 2	0·132	0·152	1·50	0·367	0·477
Enschede sand	0·380	0·431	1·60	0·320	0·411
Hoherstall Waalre	0·341	0·400	1·58	0·350	0·450
Oostelijke rivierenzand	0·233	0·307	2·06	0·322	0·423
Itterbeck 330 μm	0·342	0·410	1·60	0·337	0·434
Itterbeck 125–250 μm	0·219	0·278	1·71	0·345	0·465
Itterbeck mixture 1	0·162	0·223	2·43	0·333	0·450
Itterbeck mixture 2	0·143	0·203	3·17	0·319	0·440
Sterksel	0·228	0·300	2·25	0·357	0·474

*Minimum and maximum porosity are obtained using a column with the same preparation method as that described in the 'Experimental set-up' subsection.

Table 4. Overview of new experiments

Exp. no.	Sand type	k: m/s	RD	W: m	L: m	D: m	Ø: mm	H_c: m*	H_c/L
B132	Baskarp 1	$9{\cdot}3 \times 10^{-5}$	0·65	0·300	0·344	0·100	6	0·065	0·189
B133	Baskarp 1	$9{\cdot}5 \times 10^{-5}$	0·65	0·300	0·344	0·100	6	0·065	0·189
B115	Baskarp 1	$5{\cdot}4 \times 10^{-5}$	0·89	0·300	0·344	0·100	6	0·080	0·233
B118	Baskarp 1	$6{\cdot}3 \times 10^{-5}$	0·89	0·300	0·344	0·100	6	0·080	0·233
B142	Baskarp 1	$6{\cdot}2 \times 10^{-5}$	0·91	0·300	0·344	0·100	6	0·080	0·233
B145	Baskarp 1	$8{\cdot}0 \times 10^{-5}$	0·65	0·300	0·341	0·100	12	0·069	0·202
B146	Baskarp 1	$8{\cdot}0 \times 10^{-5}$	0·65	0·300	0·341	0·100	12	0·070	0·205
B143	Baskarp 1	$5{\cdot}5 \times 10^{-5}$	0·91	0·300	0·341	0·100	12	0·084	0·246
B144	Baskarp 1	$5{\cdot}3 \times 10^{-5}$	0·91	0·300	0·341	0·100	12	0·085	0·249
W130	Hoherstall Waalre	$5{\cdot}1 \times 10^{-4}$	0·65	0·300	0·344	0·100	6	0·106	0·308
W131	Hoherstall Waalre	$5{\cdot}4 \times 10^{-4}$	0·65	0·300	0·344	0·100	6	0·086	0·250
I165	Itterbeck 125–250 μm	$1{\cdot}4 \times 10^{-4}$	0·93	0·300	0·344	0·100	6	0·096	0·279
I164	Itterbeck 125–250 μm	$1{\cdot}3 \times 10^{-4}$	0·97	0·300	0·344	0·100	6	0·113	0·328
I166	Itterbeck mixture 1	$4{\cdot}6 \times 10^{-5}$	1·00	0·300	0·344	0·100	6	0·210	0·610
I168	Itterbeck mixture 2	$2{\cdot}7 \times 10^{-5}$	0·89	0·300	0·344	0·100	6	0·205	0·596
I167	Itterbeck mixture 2	$3{\cdot}7 \times 10^{-5}$	0·93	0·300	0·344	0·100	6	0·152	0·442
O140	Oostelijke rivierenzand	$2{\cdot}0 \times 10^{-4}$	0·65	0·300	0·344	0·100	6	0·095	0·276
O141	Oostelijke rivierenzand	$2{\cdot}1 \times 10^{-4}$	0·65	0·300	0·344	0·100	6	0·090	0·262
O163	Oostelijke rivierenzand	$1{\cdot}3 \times 10^{-4}$	0·94	0·300	0·344	0·100	6	0·185	0·538
S170	Sterksel	$7{\cdot}6 \times 10^{-5}$	0·89	0·300	0·344	0·100	6	0·350	1·017
E169	Enschede sand	$3{\cdot}2 \times 10^{-4}$	0·94	0·300	0·344	0·100	6	0·090	0·262
E150	Enschede sand	$4{\cdot}1 \times 10^{-4}$	1·00	0·150	0·344	0·100	6†	0·099	0·288
Bms19	Baskarp 2	$8{\cdot}0 \times 10^{-5}$	0·94	0·881	1·385	0·403	20·5	0·210	0·152
Ims18	Itterbeck 330 μm	$3{\cdot}5 \times 10^{-4}$	0·87	0·881	1·385	0·403	20·5	0·330–0·360‡	0·238–0·260
Ims20	Itterbeck 330 μm	$3{\cdot}9 \times 10^{-4}$	0·91	0·881	1·385	0·403	20·5	0·194	0·140

*H_c refers to the head drop at which the pipe developed to the upstream side.
†Visualisation experiment with half a circular hole.
‡In this experiment the head was increased in larger steps due to time constraints: the presumed critical head is between the stated values.

experiments with Baskarp sand and reasonable in the case of the other experiments.

RESULTS AND ANALYSIS

The results of the experiments have been interpreted at different levels. At the macro-scale, the critical head was obtained in each experiment, making comparisons possible with the adjusted and original Sellmeijer models to verify the effects of scale and sand characteristics. Observations and hydraulic head measurements allowed for the analysis of pipe dimensions and hydraulics. Information about the erosion mechanism was obtained at the grain scale.

Processes observed

The sequence of processes in small-scale experiments with a small circular exit has been described by Müller-Kirchenbauer (1978) and Miesel (1978). They investigated the backward erosion phenomena in a small-scale (seepage length is 0·72 m) set-up with a circular exit, simulating a sandy layer with a considerable blanket layer. Müller-Kirchenbauer (1978) described the process in four steps.

(*a*) Fluidisation phase: fluidisation of the sand occurs near the exit.
(*b*) Transport phase: sand is transported through and out of the vertical section and a lens is formed in the sand around the exit. The process stops at a given moment.
(*c*) Backward erosion: pipes are formed that grow towards the upstream side. The process stops and a further increase in head drop is necessary to keep the pipe growing.
(*d*) After a further increase in the head, a critical level is exceeded and the pipe grows until breach.

Miesel (1978) investigated how the diameter of the exit hole affects the backward erosion process, and found that the processes are similar to the observations by Müller-Kirchenbauer (1978) but depend on the exit size. The heads required for fluidisation and grain ejection increase with exit diameter, the latter coinciding with the critical head for exit diameters larger than 13 mm, such that equilibrium in pipe formation is not observed after grain ejection. Exit diameter has hardly any effect on the critical head.

The observations in the small- and medium-scale experiments presented here resemble those of Müller-Kirchenbauer (1978) and Miesel (1978) for a small exit diameter. An important difference in the set-up is the vertical length of the circular exit, which was considerably smaller in the new experiments. Fluidisation of the sand bed occurred at a head drop of approximately 0·02–0·03 m in the small-scale experiments. The circular hole was gradually filled with sand, and sand was transported and deposited around the hole once the entire vertical section was filled with sand at a head difference of approximately 0·03–0·06 m. In the medium-scale experiments with an exit hole diameter of 20·5 mm and in the small-scale experiments with an exit hole diameter of 12 mm, only part of the sand surface boiled.

The transparent cover allowed for an analysis of the process of pipe formation. Initially pipes formed in every direction. However, after an incremental increase in the head, one or two pipes developed towards the upstream side. For the pipe to continue developing, several increases in the head were necessary, indicating that the final critical head is dominated by the process of pipe progression.

The width of the pipe tip appeared to be independent of scale and pipe length. However, the widths of the pipe tips in the relatively coarse sand types appeared to be larger than those in finer sands. The pipe width is discussed in more detail in the section on pipe analysis. Upon lengthening, secondary erosion caused the pipe to widen downstream of

the tip. Although the processes in small- and medium-scale experiments were very similar, the larger length of the pipes and the availability of width in the medium-scale experiments resulted in more pronounced meandering and widening of the pipe (Fig. 3). This concurs with the observations in experiments by Hanses (1985), where pipes with lengths in excess of 25–30 cm tended to relocate as a result of meandering.

The sensitivity of the piping process to micro-scale heterogeneity emerged from one of the medium-scale experiments (Ims18), in which the sand bed showed layering perpendicular to the direction of flow. In this experiment, the pipe developed in a direction perpendicular to the direction of the flow where it met a thin layer of coarse grains (Fig. 4). After the head was increased, the pipe broke through the coarser layer and continued to develop over a distance of several decimetres in the upstream direction until it encountered the next coarse layer. Layering was prevented in the second experiment with this type of sand (Ims20), in which the critical head proved to be significantly lower.

Experimental critical gradient analysis

The small- and medium-scale experiments were performed with different sand types, different scales and relative densities. The critical gradients obtained were compared to acquire information about the influence of soil characteristics and configuration.

Soil characteristics. The variation of sand types and density in the experiments allowed for the investigation of the impact of soil characteristics on critical gradient. Selecting the experiments with uniform sands made it possible to observe the effect of grain size. Fig. 5(b) shows the influence of grain size in uniform sands (max. $d_{60}/d_{10}=2{\cdot}25$) at different relative densities and scales, indicating that grain size has a limited impact. Dense samples tended to result in higher critical gradients. The critical gradients in two experiments were remarkably high (dense samples of Oostelijke rivierenzand and Sterksel sand). In both experiments, there was sudden rapid pipe formation after several incremental increases in the head. The experiment on Sterksel sand may have been influenced by the migration of fines through the sand bed, since the exit cylinder was found to be turbid and the results with the riser tubes indicate a fall in permeability towards the

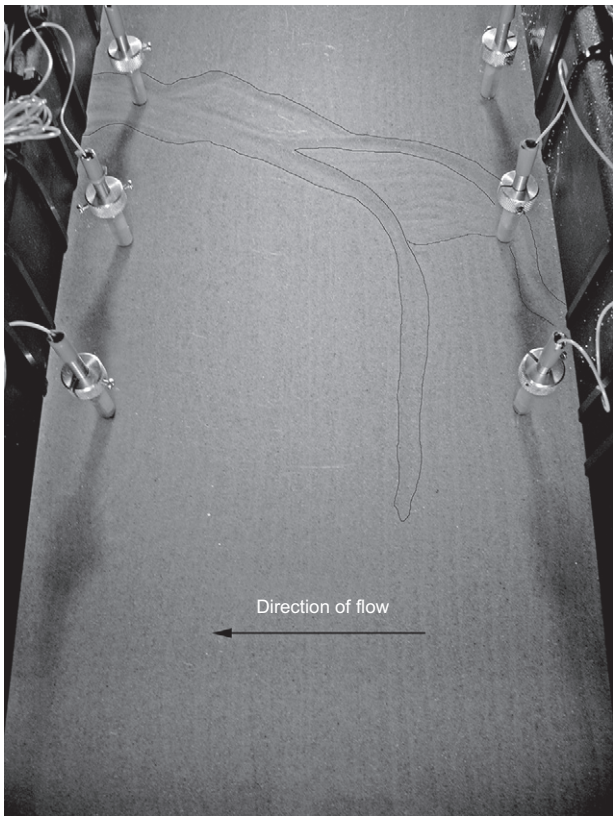

Fig. 4. Pipe formation perpendicular to the direction of flow resulting from stratification

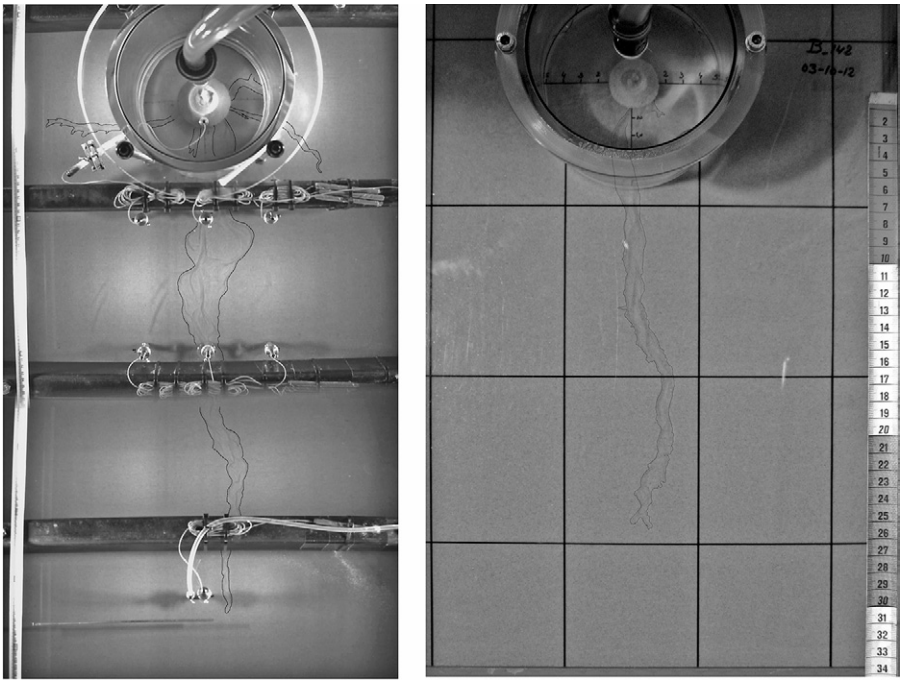

Fig. 3. Example of pipe meandering and pipe widening in a medium-scale experiment (Bms19) (left) and small-scale experiment (B142) (right). The contour of the pipe has been drawn manually

downstream exit, although bulk permeability was not particularly low. In the other experiments, the critical gradient was not closely correlated with grain size. It can be concluded that, with the uniform sand types investigated, the influence of grain size on critical gradient is limited, or compensated by other properties such as permeability.

The effect of the uniformity coefficient was investigated by mixing different uniform fractions. Fig. 5(c) shows the effect in these experiments. It should be noted that permeability is also affected by the addition of fines, which results in significantly stronger samples, indicating that the grain size distribution does affect the critical gradient. Experiments with sands containing fines require longer time intervals with a constant head than applied in the series of experiments described in this paper, since the migration of fines can be time-consuming (Moffat *et al.*, 2011). The removal of fines from the sample is known to result in a decrease in the critical gradient (Richards & Reddy, 2012).

The experiments prove that the critical gradient increases with the uniformity coefficient and relative density of the sand, whereas, in uniform samples, the critical gradient is not very much influenced by the size of the grains. However, it is difficult to be conclusive about the individual influence of grain size, uniformity coefficient and relative density on the basis of the analysis of critical gradients since these parameters cannot be varied independently. Each parameter affects the permeability of the sample. Comparing the critical gradients with predicted critical gradients using a model could further clarify this area.

Model geometry. The small-scale experiments with Baskarp sand were performed with two exit hole sizes: 6 and 12 mm. Fig. 5(a) shows the experimentally obtained critical gradients for these experiments for two different relative densities (65% and 90%): the critical gradient increased only slightly with the exit hole diameter, confirming the findings of Miesel (1978).

The critical gradients for the medium-scale experiments are lower than for the small-scale experiments, providing an indication of how scale affects critical gradient. Owing to the different ratios in sand bed thickness and seepage length, the results of Hanses (1985) and the new experiments presented in this paper cannot be compared directly in quantitative terms. However, a qualitative comparison allows for an assessment of the role played by scale, as seen in Fig. 5(d), in which the experiments are shown with the same D/L ratio (thickness sand bed/seepage length), but with a scale ratio of 4.

It should be noted that the scale effect is more marked in the experiments conducted by Hanses (1985). A possible explanation is the very small width of the sand box in the small-scale set-up (0·165 m in this experiment). On the basis of numerical calculations of the flow towards the pipe, Vandenboer *et al.* (2013) conclude that the width in small-scale experiments should be at least as large as the seepage length. As the pipe dimensions remain more or less the same at different scales, a relatively limited width might affect larger-scale experiments to a lesser extent than small-scale experiments: at comparable pipe dimensions the

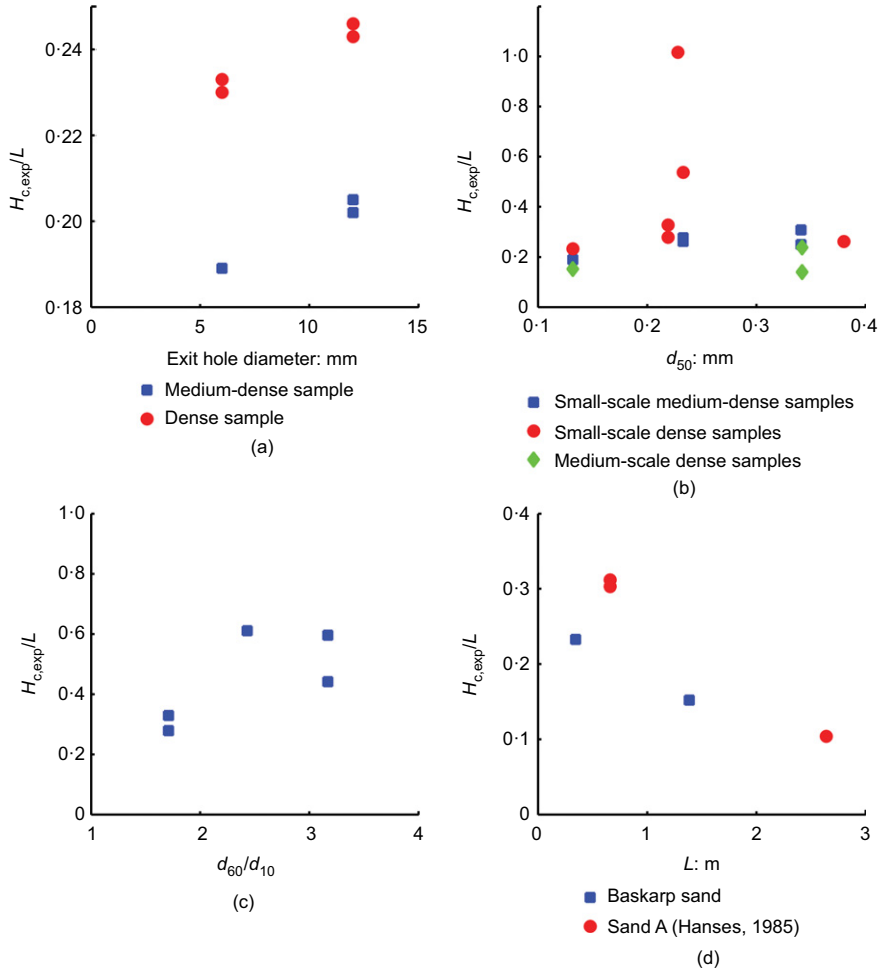

Fig. 5. Influence of soil properties and geometry on critical gradient: (a) exit hole diameter (small-scale tests); (b) grain size for uniform sand types (d_{50}); (c) uniformity coefficient (presented by d_{60}/d_{10}); and (d) scale on critical gradient (in small-scale model tests)

limited width restricts the flow towards the pipe relatively more in the case of a small box than in the case of a large box. Another explanation could be that, in the experiments by Hanses (1985), the exit hole is not scaled in line with the dimensions of the set-up. Given the conclusion stated above that the hole size has a limited effect on the critical gradient, this is not likely to be the main cause of the anomaly.

Comparison of experimental critical gradients with Sellmeijer model

As all the experiments presented here involved equilibrium in pipe development, they can be used as a basis for comparison with models predicting pipe progression such as Sellmeijer's model (Sellmeijer, 1988).

Sellmeijer's model was implemented in a 2D numerical groundwater model to account for different configurations (Sellmeijer, 2006) and used to derive a calculation rule for a 'standard levee' located on top of a homogeneous confined aquifer. The original and adjusted rules are described in Sellmeijer *et al.* (2011). The Sellmeijer model is known to result in good predictions for large-scale experiments with 2D configurations, such as the IJkdijk experiments (Sellmeijer *et al.*, 2011) and the Delta Flume experiments (Weijers & Sellmeijer, 1993). The original and adjusted rules are given in equations (1) and (2)

$$\frac{H_c}{L} = F_R F_S F_G \qquad F_R = \eta \frac{\gamma'_p}{\gamma_w \tan\vartheta} \qquad F_S = \frac{d_{70}}{\sqrt[3]{\kappa L}} \qquad F_G = 0{\cdot}91\left(\frac{D}{L}\right)^{\left\{0{\cdot}28/\left[(D/L)^{2{\cdot}8}-1\right]\right\}+0{\cdot}04} \tag{1}$$

$$\frac{H_c}{L} = F_R F_S F_G \qquad F_R = \eta \frac{\gamma'_p}{\gamma_w} \tan\vartheta \left(\frac{\mathrm{RD}}{\mathrm{RD_m}}\right)^{0{\cdot}35} \left(\frac{U}{U_m}\right)^{0{\cdot}13} \left(\frac{\mathrm{KAS}}{\mathrm{KAS_m}}\right)^{-0{\cdot}02} \qquad F_S = \frac{d_{70}}{\sqrt[3]{\kappa\, L}} \left(\frac{d_{70m}}{d_{70}}\right)^{0{\cdot}6} \qquad F_G = 0{\cdot}91\left(\frac{D}{L}\right)^{\left\{0{\cdot}28/\left[(D/L)^{2{\cdot}8}-1\right]\right\}+0{\cdot}04} \tag{2}$$

where RD denotes relative density, KAS denotes roundness of particles and subscript m denotes the mean value of the parameter in selected experiments (Sellmeijer *et al.*, 2011). As pipe formation itself is a 3D phenomenon (irrespective of whether the configuration is 2D or 3D), it was assumed that the model could also be applied to 3D configurations, which are common in practice. Prior to the present study, this assumption had not been verified experimentally.

The calculation rule, which is suited for a standard dyke geometry, was used to 'postdict' the experiments described in the present study. As the rule is fitted to the results of the numerical model, the outcomes of the rule and the numerical calculation are the same for the standard dyke geometry. When a configuration is used with an exit that deviates from the standard dyke geometry, the difference between the outcomes of the model and the rule should be examined. The present experiment was therefore numerically simulated in two dimensions, with the exit hole being represented by a gap of infinite length and width equal to the exit hole diameter. It is not yet possible to assess the influence of a 3D configuration on critical gradient.

Figure 6 shows the expected influence of the exit hole diameter on the calculated critical head using the 2D numerical model for one of the experiments. As the influence of diameter on critical head is relatively small in the studied range, it is considered acceptable to use the rule rather than the 2D numerical model to 'postdict' the experiments. It should be noted that KAS (grain angularity) is a very minor factor and this parameter was therefore not taken into account. The difference in the angularity of the tested sand types is also relatively small.

Figure 7 shows both the experimental and calculated critical gradients for all experiments using the original and adjusted calculation rules. It is immediately clear that the calculated critical gradients are approximately two times larger than the experimentally obtained values. Apparently, the 3D configuration results in considerably lower critical gradients than a 2D configuration, for which the model has been validated. The 2D model cannot predict the 3D groundwater flow conditions, which apparently play a major role. Despite this, the comparison with the model is useful as a way of identifying the effect of other properties.

Figure 8 displays the results of those experiments in which the soil type and relative density were varied. The predicted critical gradients obtained with the original and adjusted rules were comparable in Baskarp sand experiments; variations were found mainly with coarser sands. The graphs show that the variation was more or less the same for all Baskarp experiments, indicating that the model accounts well for the influence of permeability and scale. The comparison of experiments with the Sellmeijer models did not establish a clear trend with respect to grain size.

Like the experiments with Oostelijke rivierenzand and Sterksel sand, the experiments in which fines were added indicated relatively high critical gradients by comparison with the uniform sands. The Sellmeijer model does

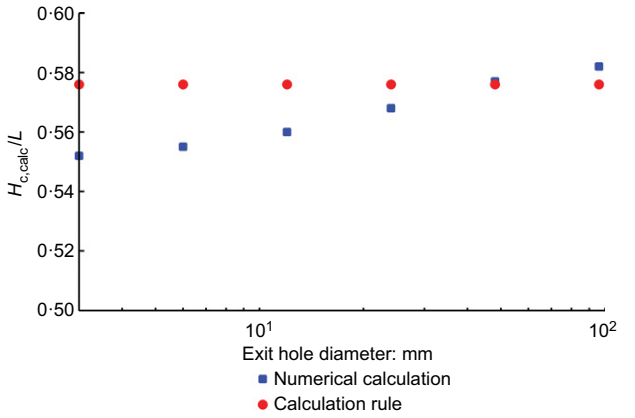

Fig. 6. Calculated critical gradients for different hole diameters comparing the outcome of the 2D numerical calculation and the calculation rule (using experiment B115 as an example)

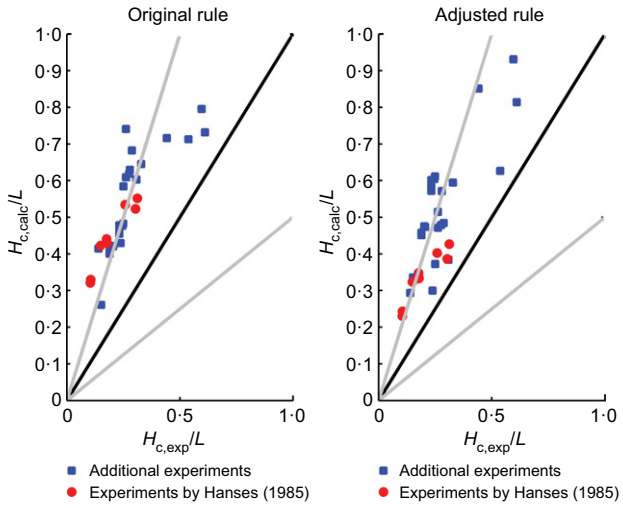

Fig. 7. Experimental and calculated critical gradients for all available experiments (lines in black and grey indicate lines where there is no variation (1:1) and variation by a factor of 2 (1:2, 2:1), respectively

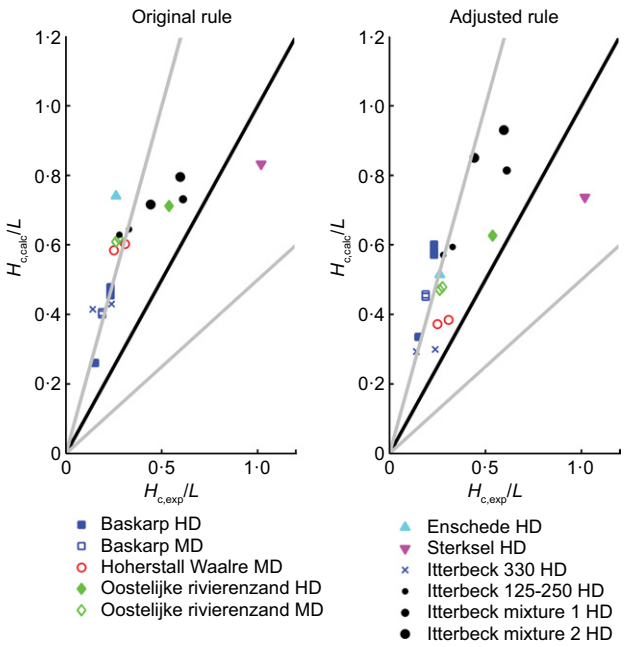

Fig. 8. Experimental and calculated critical gradients in experiments investigating sand type and relative density (lines in black and grey indicate lines where there is no variation (1:1) and variation by a factor of 2 (1:2, 2:1), respectively (MD: medium density; HD: high density)

not predict this improvement in strength accurately. Neither model captures all variations correctly.

The comparison of experimentally obtained critical gradients with the gradients calculated with the Sellmeijer rules gives several insights: the variation is approximately a factor of 2 for both small- and medium-scale experiments with fine uniform sands, indicating that the Sellmeijer model overpredicts the critical gradient in a 3D configuration. The effects of scale and model size ratios are predicted quite well. The outliers indicate that certain processes or parameters that are currently not included in the model have a major impact on the critical head. The experimental results were not conclusive but they indicate that these outliers can be found for samples in which fines transport and high relative density are features. The lack of a match between experiments and predictions emphasises the need for the development of a new model.

Pipe analysis

Looking at the critical head in experiments does not identify the causes of any differences found between model and experiment, or establish why adjustments were found to be necessary in the Sellmeijer model (Sellmeijer *et al.*, 2011). A possible explanation might be found in the pipe dimensions and hydraulics.

In all experiments, the process of pipe formation could be observed through the transparent cover. The pipe dimensions provided valuable information about erosion at the tip of the pipe (primary erosion) and secondary erosion resulting in widening of the pipe. In some experiments (selected experiments by Hanses (1985), medium-scale experiments and visualisation experiment), riser tubes were placed in the cover of the set-up to measure the hydraulic heads in the pipe. The impact of the pipe on the groundwater flow is important in terms of modelling the mechanism.

Pipe width. Hanses (1985) analysed the pipe dimensions and concluded that the pipe width near the tip was constant in all experiments (performed with one sand type: sand A) at approximately 15–20 mm. However, analysis of the drawings of pipe formation in these experiments showed that this is an overestimation of the pipe width at the tip. The tip width was defined here as the width of the pipe where it becomes more or less constant: approximately 1–2 cm behind the tip. The average tip width was found to be 13·7 mm in all available pipe drawings, which is about 42 times the average grain diameter.

The pipe dimensions were analysed for the newly performed small- and medium-scale experiments (Fig. 3). The contour of the pipe was drawn to include several lengths ($1/4\,L$, $1/3\,L$, $1/2\,L$ and $3/4\,L$), after which the sizes of the tip, centre section and tail of the pipe were estimated. The tip width, which was found to be more or less constant upon lengthening, was averaged for the pipe lengths of $1/4\,L$, $1/3\,L$ and $1/2\,L$. At a length of $3/4\,L$, the equilibrium head was presumably exceeded, possibly resulting in unreliable values.

Figure 9 (left-hand figure) shows the average pipe widths as a function of d_{50} for all available experiments. Although the method used to estimate pipe widths was not exact, a relationship was observed between pipe width and grain size. The width of the tip of the pipe was found to be fairly constant for each soil type at approximately 30 grains in most of the small-scale experiments. No relation was found between exit hole size and pipe width, or between relative density and

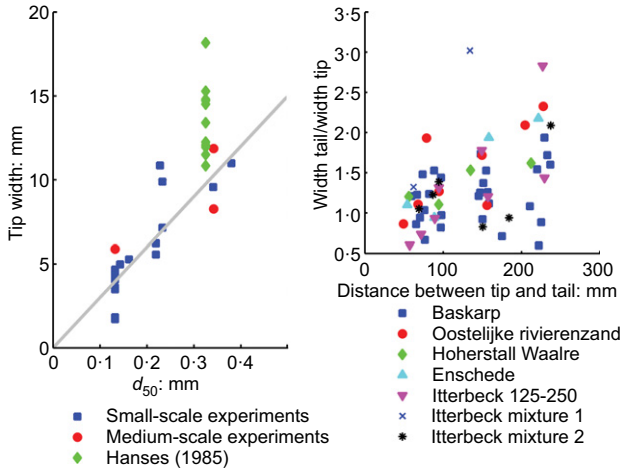

Fig. 9. Tip width as a function of the mean grain size (grey line indicates a width of 30 grains) (left) and degree of widening (ratio of tail width to tip width) as a function of the measured distance between tip and tail in various small-scale experiments (right)

pipe width. The widths observed in some experiments were significantly different from the others. Not all variations can be explained: experiments that were identical in terms of set-up, relative density and critical gradient may result in different pipe widths. In some experiments, it was possible to explain variations. For example, the large observed width in experiment S170 (d_{50} 0·228 mm) can be explained by the large critical gradient that was required in this experiment.

The tip widths obtained from experiments by Hanses (1985) are all relatively large. A possible explanation is the difference in the cover. The cover in all the new experiments described in this paper was coated on the inside with silicone to ensure a rough clay-like surface, while the cover in the experiments by Hanses was smooth. It should also be noted that, in the selected Hanses experiments, drawings of the pipe were available for only one pipe length.

As already noted in the description of the piping process, the pipes widen downstream of the tip as a result of secondary erosion. The extent of widening was estimated by measuring the increase in the pipe width from tip to tail. Fig. 9 (right-hand figure) shows the degree of widening (defined here as the ratio of tail width to tip width) as a function of pipe length in the small-scale experiments. Owing to the severe meandering, the medium-scale experiments are less suitable for an analysis of this kind. Fig. 9 (right-hand figure) shows that there is no correlation between the degree of widening of the pipe and grain size.

On average the degree of widening increases with pipe length, but there is considerable scatter and, in various cases, the tail is actually not as wide as the tip. It should be noted that, at larger pipe lengths, the pipe was not in equilibrium and so the final shape of the pipe corresponding to the hydraulic load was probably not reached. More accurate results could be obtained by measuring the pipe width along its entire length.

As the degree of widening was comparable for all considered grain sizes and the pipe tip width increased with grain size, it is concluded that the pipes of sands with larger grain sizes are wider in general.

Pipe gradient. Both primary and secondary erosion are affected by the impact of the pipe on the groundwater flow pattern. The Hagen–Poiseuille equation states that the hydraulic gradient in the pipe depends on the size of the pipe and on the flow through the pipe. The size of the pipe is determined by secondary erosion and the flow through the pipe is mainly determined by the scale of the set-up, the permeability and hydraulic head difference in the sample. The flow velocity and gradient near the tip of the pipe also depend on the gradient in the pipe. The hydraulic head distribution in the pipe has been measured in a few experiments.

In selected experiments by Hanses (1985) the hydraulic head in the pipe was measured for a pipe length that was expected to be close to the critical pipe length. At this length, the head was brought back to 0 and gradually reapplied so that the head distribution in the pipe could be measured by riser tubes. The measurements indicated a linear decrease in the hydraulic head in the pipe until close to the exit. The pipe gradient was obtained by extrapolating the head distribution at lower head drops.

In the present experiment E150 the pipe gradient was determined in a similar way for two pipe lengths: 0·175 m and 0·235 m. It should be noted that these pipe lengths are presumably larger than the critical pipe lengths and so the pipe was not in equilibrium. It is possible that the width of the pipe did not develop fully due to ongoing erosion at the tip of the pipe. As a result the gradient in the pipe may be slightly larger than a fully eroded pipe in equilibrium.

In the medium-scale experiments – Bms19 and Ims20 – equilibrium was observed several times and the pipes developed in the path of the pore pressure transducers, allowing the hydraulic head in the pipes to be measured. The average pipe gradients at equilibrium head (obtained by a linear least-squares regression of measured hydraulic heads in the pipe) are listed for each experiment in Table 5.

The effect of the soil type on pipe gradient was established by comparing the medium-scale experiments (Fig. 10, left). The pipe gradient in Baskarp sand is considerably higher than the pipe gradient in Itterbeck sand, although the critical heads are comparable. This corresponds well with the observation that pipe width is larger in coarser sands.

Enschede sand, Itterbeck 330 um and sand A are comparable, all being uniform medium-grained sands. Nevertheless, the pipe gradients varied significantly. Differences in pipe gradient therefore originate from differences in hydraulic head, scale and configuration. Since the process of secondary erosion is driven by flow through the pipe, erosion should increase with the flow exiting through the hole in the case of a pipe with dimensions equal to the tip width. More erosion results in larger pipes and consequently lower pipe gradients. Fig. 10 (right) shows the measured pipe gradients as a function of corresponding flow. Indeed, a decrease in the pipe gradient with increasing flow was observed in all of the present authors' experiments. It is remarkable that the relatively high pipe gradient for the medium-scale experiments with Baskarp sand can be fully explained by the relatively low flow resulting from the lower permeability of the sand. The relationship between flow and pipe gradient is an indicator of the influence of secondary erosion on the pipe gradient.

Table 5. Average pipe gradients (p) and measured flow (Q_{exp}) in equilibrium conditions in various experiments

Experiment	Sand type	d_{50}: mm	l: m	H: m	p	Q_{exp}: m^3/s
26a	Sand A	0·325	0·250	0·130	0·089	$3·98 \times 10^{-6}$
53	Sand A	0·325	0·165	0·214	0·092	$2·01 \times 10^{-6}$
73	Sand A	0·325	0·615	0·298	0·060	$1·32 \times 10^{-5}$
E150	Enschede	0·380	0·175	0·093	0·131	$3·22 \times 10^{-7}$
E150	Enschede	0·380	0·235	0·079	0·119	$1·45 \times 10^{-6}$
Bms19	Baskarp	0·132	0·440	0·149	0·096	$2·16 \times 10^{-6}$
Bms19	Baskarp	0·132	0·480	0·159	0·093	$2·35 \times 10^{-6}$
Bms19	Baskarp	0·132	0·520	0·170	0·095	$2·58 \times 10^{-6}$
Bms19	Baskarp	0·132	0·690	0·179	0·088	$2·95 \times 10^{-6}$
Bms19	Baskarp	0·132	0·940	0·187	0·089	$3·31 \times 10^{-6}$
Bms19	Baskarp	0·132	1·135	0·203	0·108	$3·81 \times 10^{-6}$
Ims20	Itterbeck 330 μm	0·283	0·647	0·175	0·059	$1·14 \times 10^{-5}$
Ims20	Itterbeck 330 μm	0·283	0·742	0·162	0·038	$1·17 \times 10^{-5}$
Ims20	Itterbeck 330 μm	0·283	1·197	0·170	0·065	$1·54 \times 10^{-5}$

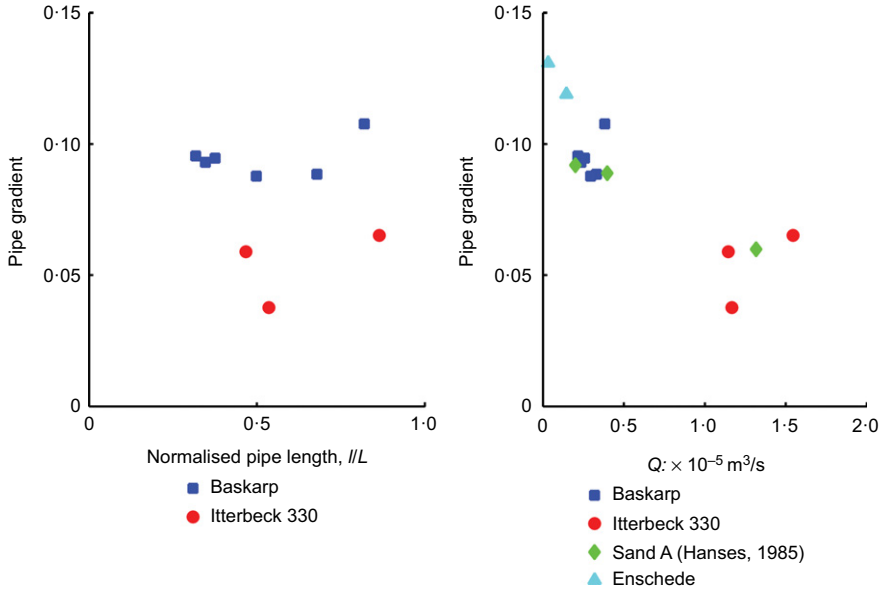

Fig. 10. Pipe gradient as a function of (left) normalised pipe length (l/L) and (right) measured flow

Pipe depth. A series of experiments was performed with a transparent side wall and the exit hole situated along the wall in order to visualise the erosion mechanism. However, the pipe developed partly alongside the wall in only one of the experiments (E150). The erosion mechanism near the tip was not visible in this experiment, but the pipe depth could be determined where the pipe developed along the wall: the pipe depth varied and the observed maximum was 2·3 mm, approximately six times the mean grain size. Fig. 11 shows the pipe where it coincides with the wall. This section was studied during the pipe development of 0·235 m to 0·343 m and, although grain transport was visible, the depth remained unchanged in this interval, as is shown by the images for two different pipe lengths.

The pipe depth was also analysed in one of the regular small-scale experiments (I167). Once the pipe reached the upstream level, the tap was closed and the cover was removed to expose the top of the sand bed. The pipe dimensions were then recorded using laser equipment (the position of the sand surface was measured in a grid of 456×225 data points). Fig. 12 shows the resulting pipe geometry.

Although the measurement was taken at the end of the test, analysis of the pipe dimensions provides an indication of the depth of the pipe and its slope angles. Fig. 13 shows the cross-section of the pipe at various distances from the upstream filter. This figure shows that the pipe depth varies along the width of the pipe, with larger depths in the eroding sides of the pipe bends. The maximum depth observed in these cross-sections was 3·5 mm, which is 24 times the mean grain diameter. In most cross-sections, the pipe was shallower: approximately 1–2 mm (7–14 times the grain diameter). No distinct depth increase was observed towards the pipe tail.

The slopes of the side walls of the pipe were evaluated; in most cases, they were well below the slope corresponding to the expected friction angle. It was only at one location, where the flow seemed to create erosion in the corner (at $x = 180$ mm in Fig. 12), that the slope of the eroding side wall was 40°.

Müller-Kirchenbauer (1978) and Van Beek *et al.* (2014b) studied pipe depth by evaluating the volume of sand that was ejected to the surface. They found that the average depth remained constant during lengthening. Van Beek *et al.* (2014b) calculated the average depth to be approximately

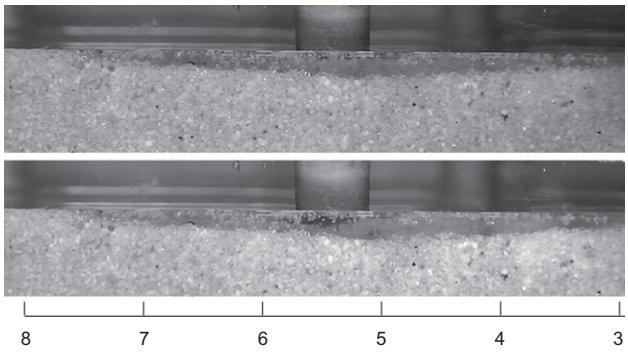

Fig. 11. Visible part of the pipe at 3 to 8 cm from the exit hole, at a pipe length of 250 mm (top figure, taken at test time of 373·45 min, head drop 8 cm) and 280 mm (bottom figure, taken at test time of 375·58 min, head drop 8 cm)

2·6 mm for an experiment on Oostelijke rivierenzand, which is 11 times the mean grain diameter. Hanses (1985) estimated the pipe depth to be approximately 1·5–2 mm, which is 5–6 times the mean diameter of the sand.

DISCUSSION OF THE EROSION MECHANISM

The erosion mechanism that causes the pipe to lengthen and widen is the basis for the prediction of pipe progression and it is therefore essential to understand this mechanism properly. Analysis of the experiments presented in this paper provides valuable information about the erosion mechanism that can serve as a basis for a new and more complete model.

Observed erosion mechanisms

The experiments show that both 'primary erosion' and 'secondary erosion' are important for the prediction of piping, as will be explained below.

A first indicator of the importance of primary erosion was found in the experiment in which the sand bed was layered (Ims18), resulting in pipe formation perpendicular to the direction of flow when a slightly coarser layer was encountered. The fact that such a small variation in grain size can

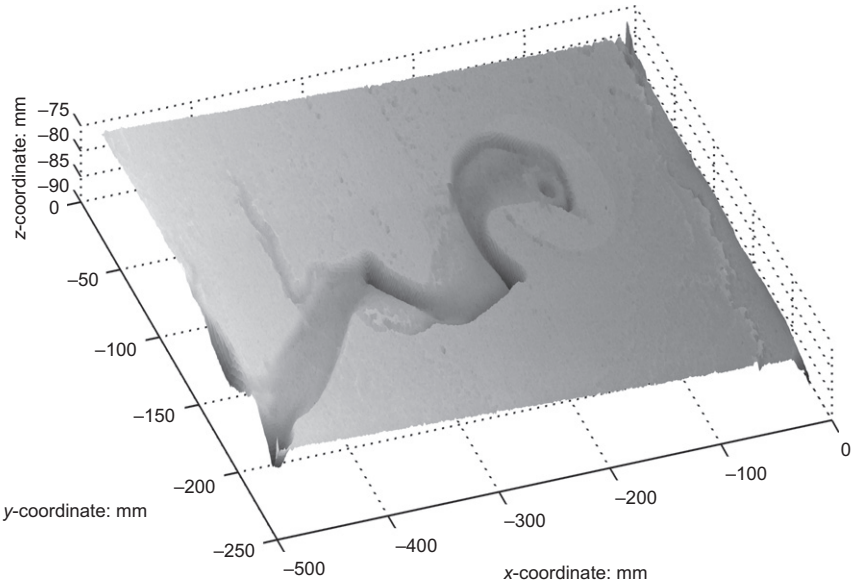

Fig. 12. Pipe geometry in experiment I167

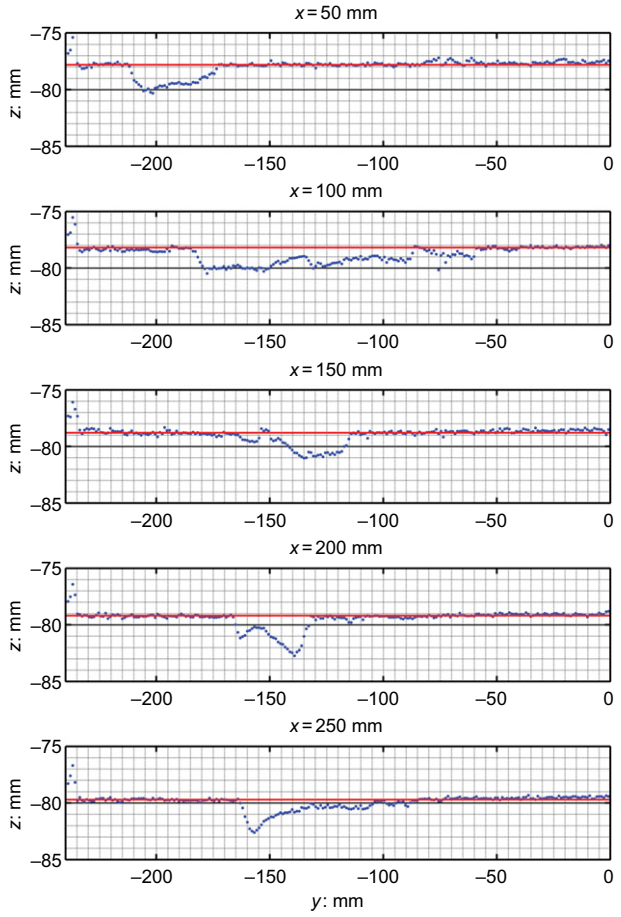

Fig. 13. Cross-sections of the pipe at various distances from the upstream filter

stop lengthening is a strong indication that a resistance needs to be overcome near the tip of the pipe to facilitate pipe progression. In addition, the width of the pipe tip proves to be independent of scale or pipe length. A possible explanation of this constant width is that the hydraulic load at the tip of the pipe needs to overcome the resistance for a certain group of grains. This corresponds to the findings of Hanses (1985) and Townsend *et al.* (1988), who observed the intermittent transport of groups of grains at the pipe tip. Another important finding is that the tip width of the pipe was found to increase with grain size and to be independent of scale: the width of the pipe tip was approximately 30 grains. This suggests that the area in which the sand resistance needs to be overcome is larger for sands with larger grain sizes. This concurs with recent studies of pipe initiation, which found that a group of at least 20 grains needs be transported to initiate a pipe, irrespective of grain size and the scale of the set-up (Van Beek *et al.*, 2014a).

If, indeed, primary erosion determines pipe lengthening, the relevance of secondary erosion becomes clear at once. Secondary erosion affects the hydraulic gradient in the pipe, which in turn determines the hydraulic conditions near the tip of the pipe. Indeed, secondary erosion was also observed in the experiments. In all experiments, the pipe width near the tail increased upon lengthening. Photographs and the measured pipe geometry in Fig. 13 show the meandering of the pipe, resulting in scouring in the outer bend of the pipe. The scour results in the lateral widening of the pipe, while an increase in depth was not found. Furthermore, a relationship was found between pipe gradient and flow, indicating that the pipe size adjusts to convey the amount of water transported through the pipe.

Both erosion mechanisms should therefore be taken into account to model the progression of the pipe correctly. This has not yet been done so far: Schmertmann (2000) neglected the influence of the pipe on the groundwater flow; Sellmeijer (1988) and Sellmeijer *et al.* (2011) neglected the process of primary erosion. The concept of combining primary and secondary erosion to predict backward erosion piping is therefore novel.

Influence of primary and secondary erosion on critical gradient

A combination of these mechanisms may explain why the critical gradient is not extensively affected by grain size (in uniform sands). The present authors suggest here that a group of grains at the tip of the pipe needs to be fluidised by a local critical hydraulic gradient (i_c) at the tip of the pipe. The tip of the pipe is a singular point and so, theoretically, the local gradients near the pipe tip will go to infinity. Although the continuum approach is not infinitely valid in practical

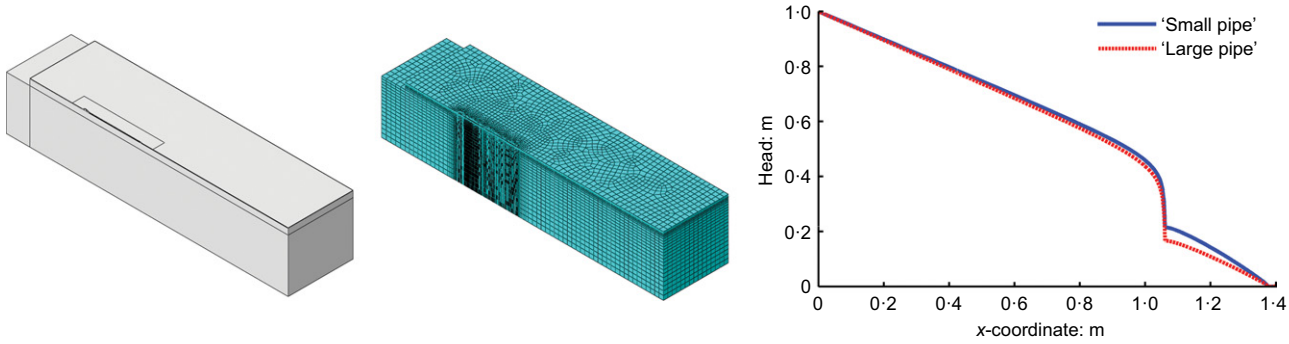

Fig. 14. Configuration, mesh and potential distribution along the centre axis of symmetrical 3D numerical simulations of the medium-scale experiments (van Beek *et al.*, 2014b). Pipes have been simulated by adding a permeable zone in the centre of the sand sample, located at 1·06 to 1·385 m. Permeability in the pipes differs for the continuous line and the dotted line, representing a pipe with a large impact (dotted line), as would be the case for a coarse sand, and a pipe with a smaller impact (continuous line), as would be the case with a fine sand

terms, the gradient does increase towards the pipe tip. Fig. 14 illustrates examples of potential distribution in 3D sand samples, including pipes with different impacts on the groundwater flow. The sharp decrease in potential near the pipe tip illustrates the concentration of flow lines. Upon approaching the tip, the gradient reaches a very high value and, at this point, the continuum approach is no longer valid.

A practical approach to deal with the singularity would be to consider the gradient across a group of grains, as when predicting pipe initiation (Van Beek *et al.*, 2014a). The constant size of the pipe tip width (of approximately 30 times the mean grain diameter), as observed in the experiments, supports such an approach. For the pipe to progress, the local gradient i at some distance from the tip must exceed a critical value i_c. In the case of relatively large grains, the tip of the pipe is wider in absolute terms and it therefore requires fluidisation in a relatively large area in front of the pipe tip. Given the rapid decrease in the local gradient i with distance from the pipe tip, as illustrated in Fig. 14 by the slope of the potential, a relatively large overall gradient (H_c/L) is required to reach a critical value i_c for this local gradient. Taking primary erosion alone into account would therefore suggest that the critical head is larger for coarse sand types.

However, due to the larger size of the pipe and the consequent secondary erosion, the gradient in the pipe is relatively low for the coarser sand type, such that the local gradient in the sand upstream of the pipe and at the pipe tip is relatively high for a given hydraulic head. These two effects can counteract one another so that the net influence of grain size on critical head is limited. This is illustrated in Fig. 14, which shows the examples of relatively fine and coarse sands at critical head. The figure is based on numerical 3D simulations of the medium-scale experiments including a pipe (Van Beek *et al.*, 2014b). The fine sand has a relatively large pipe gradient due to its limited size, whereas the gradient for the coarse sand is lower. The average and local gradients will therefore be higher in the sand layer upstream of the pipe for the coarser sand (in the example in Fig. 14, the gradients upstream of the pipe were found to be up to 12% higher for the line representing coarse sand than for the line representing fine sand). This means that, despite the fact that the average gradient (H/L) is the same for both sand types in this example, the local gradients in front of the pipe are higher for the coarse sand, which allows a larger area to be fluidised in front of the pipe.

The influence of relative density on the critical gradient follows qualitatively from both primary and secondary erosion. Dense samples will be less permeable, reducing the flow in the pipe. This will lead to limited scour in the pipe and so the pipe gradient will be relatively high accordingly, requiring a relatively high overall head to cause primary erosion. In addition, the fluidisation of the pipe tip will require a relatively high gradient given the low porosity and dilatancy of the sand sample due to expansion.

The uniform sand samples resulted in a lower critical gradient than those with added fines. Although non-uniform samples require additional research, the major impact on the critical gradient can be explained theoretically by reference to primary and secondary erosion. The main difference between uniform and non-uniform samples is their permeability, which decreases with increasing fine content. At equal overall gradients and comparable mean grain size, flow velocities in the pipe are higher in the uniform sample, resulting in more secondary erosion and consequently lower pipe gradients. Accordingly, the pipe will progress at a relatively lower head in the case of the uniform sample.

A large increase in strength resulting from the variation in grain size, as encountered in the layered sand sample in one of the medium-scale experiments, can be explained by reference to primary erosion. Layers with relatively coarse grains form a barrier since a larger zone needs to be fluidised in front of the pipe tip for the pipe to progress through these layers.

Discussion of future developments

Further research should focus on the establishment of a criterion that determines the onset of erosion near the pipe tip. The experiments will have to be simulated numerically for this purpose in order to determine the local gradients around the pipe tip that cause the pipe to progress. The loosening of grains in front of the pipe tip and arching may need to be taken into account when determining a criterion of this kind. The simulation of experiments with a layered sand sample is of particular interest since layering is commonly encountered in sand layers in the field and has been found to result in large critical gradients by comparison with homogeneous equivalents. Additional experiments with layered sand beds are recommended to confirm the observed effects. Modelling of secondary erosion will be required to determine the gradient in the pipe, as shown in Fig. 14. The pipe gradient is determined by the initial pipe size (width of approximately 30 grains) and by the subsequent erosion of its walls and bottom. The literature describes criteria for incipient motion in laminar flow, which, in combination with equations for pipe flow and groundwater flow, could result in an estimate of the pipe gradient at which the grains are in a limit-state equilibrium. The applicability of the criteria for incipient

motion to erosion pipes should be investigated. The criteria implemented currently for bed erosion may not fully explain the erosion of the walls of the pipe that results in lateral widening.

The combination of these two mechanisms will lead to a novel model that can take into account the influence of scale and sand properties and heterogeneity in the path of the pipe. It has the potential to explain the influence of coarse-grained 'barriers' on critical head, which is essential for the prediction of piping in practice. A model of this kind would also make possible the development of more practical rules for specific configurations.

CONCLUSIONS

Small- and medium-scale experiments were performed and analysed to study the progression of the pipe. A circular exit led to pipe initiation at a relatively low head by comparison with experiments with other exit configurations (Van Beek *et al.*, 2014a) and equilibrium in pipe formation was observed, requiring an increase in head for pipe progression so that this process could be studied.

The critical heads obtained in the experiments, as well as those obtained from literature, were compared with the results of the Sellmeijer model (Sellmeijer *et al.*, 2011), which was developed to predict the critical head for pipe progression. Although the adapted Sellmeijer model predicts critical gradients well for 2D large-scale experiments with fine- to medium-grained sands, the present authors found that 3D configurations with flow towards a single point result in significantly smaller critical gradients than those predicted by the model. Although, in practice, the exit type may not have such a strong influence, due to the formation of multiple pipes and seepage through the cover layer and towards the hinterland, the worst-case scenario of the development of a single pipe in a configuration similar to that in the laboratory should be taken into account. In both the small- and medium-scale experiments, the model overestimates the critical head in the experiments by a factor of approximately 2.

In order to find a possible explanation for the observed variations, the pipe width, depth and gradient were analysed in detail. The findings illustrate the importance of both primary and secondary erosion. Primary erosion, which is the erosion at the tip causing the lengthening of the pipe, determines its progress, as illustrated by one of the experiments in which the pipe developed perpendicular to the flow direction when a slightly coarser layer was encountered. The finding that the width of the pipe tip increases linearly with grain size, and that it is approximately 30 times the mean grain diameter irrespective of scale or uniformity coefficient (within the studied range) supports the idea that a group of grains at the pipe tip needs to be fluidised for the pipe to progress. Secondary erosion is of importance as well: it determines the pipe gradient, which was found to be different for different sand types. The observation that flow through the pipes caused the pipe to widen towards its tail, causing lateral widening, is the main evidence underlying this conclusion. The relation between flow and pipe gradient (Fig. 10, right) further supports this idea.

A novel model should be developed that takes primary and secondary erosion into account. Further research should focus on the 3D analysis of the pipe, taking a local critical gradient upstream of the pipe tip into consideration as an additional requirement for pipe progression. The process of secondary erosion should be studied in more detail because it was found that the pipe widens, whereas deepening was not observed.

ACKNOWLEDGEMENTS

The research is part of the programme 'Research and development of flood defense assessment tools WTI2017' funded by Rijkswaterstaat – Centre for Water Management – on behalf of the Dutch Ministry of Infrastructure and the Environment.

NOTATION

D	sand sample thickness
d	height, representing the thickness of the confining layer
d_x	grain diameter at which x% of sample (by weight) is finer
F_G	geometrical shape factor
F_R	resistance factor
F_S	scale factor
H	head drop across sand sample or embankment
H_c	critical head drop across sand sample or embankment, at which ongoing erosion occurs
H_i	minimum head drop across sand sample or embankment at which pipe initiates
H_p	minimum head drop across sand sample or embankment at which pipe progresses, assuming the presence of a short pipe
k	permeability coefficient
KAS	parameter describing the roundness of particles
KAS_m	mean value of KAS in selected experiments (49·8)
L	length of seepage
l	pipe length
p	pipe gradient
Q	flow
RD	relative density
RD_m	mean value of RD in selected experiments (72·5%)
U	uniformity coefficient (d_{60}/d_{10})
U_m	mean value of U in selected experiments (1·81)
W	sand sample width
γ'_p	buoyant unit weight of particles
γ_w	unit weight of water
η	White's constant
θ	bedding angle of sand
κ	intrinsic permeability
μ	dynamic viscosity
$Ø$	exit hole diameter

REFERENCES

Bligh, W. G. (1910). Dams barrages and weirs on porous foundations. *Engng News* **64**, No. 26, 708–710.

Hanses, U. (1985). *Zur Mechanik der Entwicklung von Erosionskanälen in geschichtetem Untergrund unter Stauanlagen*. Dissertation, Grundbauinstitut der Technischen Universität Berlin, Berlin, Germany (in German).

Lane, E. W. (1935). Security from under-seepage masonry dams on earth foundations. *Trans. Am. Soc. Civ. Engrs* **100**, No. 1, 929–966.

Mansur, C. I., Postol, G. & Salley, J. R. (2000). Performance of relief well systems along Mississippi river levees. *J. Geotech. Geoenviron. Engng* **126**, No. 8, 727–738.

Miesel, D. (1978). Rückschreitende Erosion unter bindiger Deckschicht. In *Baugrundtagung*, pp. 599–626. Essen, Germany: Deutschen Gesellschaft für Erd- und Grundbau e.V. (in German).

Moffat, R., Fannin, J. & Garner, S. J. (2011). Spatial and temporal progression of internal erosion in cohesionless soil. *Can. Geotech. J.* **48**, No. 3, 399–412.

Müller-Kirchenbauer, H. (1978). Zum zeitlichen Verlauf der rückschreitenden Erosion in geschichtetem Untergrund unter Dämmen und Stauanlagen. *Verfahren der Talsperrensymposium*, Munich, Germany (in German).

Pietrus, T. J. (1981). *An experimental investigation of hydraulic piping in sand*. Masters thesis, Department of Civil Engineering, University of Florida, Gainesville, FL, USA.

Richards, K. S. & Reddy, K. R. (2012). Experimental investigation of initiation of backward erosion piping in soils. *Géotechnique* **62**, No. 10, 933–942, http://dx.doi.org/10.1680/geot.11.P.058.

Schmertmann, J. H. (2000). The non-filter factor of safety against piping through sands. In *Judgment and innovation* (eds F. Silva and E. Kavazanjian), geotechnical special publication no. 111, pp. 65–132. Reston, VA, USA: American Society of Civil Engineers.

Sellmeijer, J. B. (1988). *On the mechanism of piping under impervious structures*. Doctoral dissertation, Technische Universiteit Delft, Delft, the Netherlands.

Sellmeijer, J. B. (2006). Numerical computation of seepage erosion below dams (piping). In *Proceedings of the 3rd international conference on scour and erosion*, pp. 596–601. Gouda, the Netherlands: CURNET.

Sellmeijer, J. B., Lopéz de la Cruz, J., Van Beek, V. M. & Knoeff, J. G. (2011). Fine-tuning of the piping model through small-scale, medium-scale and IJkdijk experiments. *Eur. J. Environ. Civ. Engng* **15**, No. 8, 1139–1154.

Silvis, F. (1991) *Verificatie piping model: Proeven in de Deltagoot*. Delft, the Netherlands: Grondmechanica Delft.

Townsend, F. C. D., Bloomquist, D., Shiau, J. M., Martinez, R. & Rubin, H. (1988). *Evaluation of filter criteria and thickness for mitigating piping in sand*. Gainesville, FL, USA: Department of Civil Engineering, University of Florida.

USACE (US Army Corps of Engineers) (1956). *Investigation of underseepage and its control – Lower Mississippi river levees*, technical memorandum no. 3-424, vol 1. Vicksburg, MS, USA: Waterways Experiment Station, USACE.

Van Beek, V. M., Knoeff, J. G. & Sellmeijer, J. B. (2011). Observations on the process of backward piping by underseepage in cohesionless soils in small-, medium- and full-scale experiments. *Eur. J. Environ. Civ. Engng* **15**, No. 8, 1115–1137.

Van Beek, V. M., Bezuijen, A. & Sellmeijer, H. (2013). Backward erosion piping. In *Erosion in geomechanics applied to dams and levees* (ed. S. Bonelli), pp. 193–269. London, UK: ISTE; Hoboken, NJ, USA: Wiley.

Van Beek, V. M., Bezuijen, A., Sellmeijer, J. B. & Barends, F. B. J. (2014a). Initiation of backward erosion piping in uniform sands. *Géotechnique* **64**, No. 12, 927–941, http://dx.doi.org/10.1680/geot.13.P.210.

Van Beek, V. M., Vandenboer, K. & Bezuijen, A. (2014b). Investigation of the backward erosion mechanism in small scale experiments. In *Physical modelling in geotechnics* (eds C. Gaudin and D. White), pp. 855–861. London, UK: Taylor & Francis Group.

Vandenboer, K., Van Beek, V. M. & Bezuijen, A. (2013) 3D FEM simulation of groundwater flow during backward erosion piping. In *Proceedings of the 5th young geotechnical engineers' conference* (eds Y.-J. Cui, F. Emeriault, F. Cuira, S. Ghabezloo, J.-M. Pereira, M. Reboul, H. Ravel and A. M. Tang), pp. 301–306. Amsterdam, the Netherlands: IOS Press.

Vrijling, J. K., Kok, M., Calle, E. O. F., Epema, W. G., van der Meer, M. T., van den Berg, P. & Schweckendiek, T. (2010). *Piping – realiteit of rekenfout?*, Technical report. Utrecht, the Netherlands: Dutch Expertise Network on Flood Protection (ENW) (in Dutch).

Weijers, J. B. A. & Sellmeijer, J. B. (1993) A new model to deal with the piping mechanism. In *Filters in geotechnical and hydraulic engineering* (eds J. Brauns, U. Schuler and M. Heibaum), pp. 349–355. Rotterdam, the Netherlands: Balkema.

Yao, Q., Xie, J., Sun, D. J. & Zhao, J. (2009) *Data collection of dike breach cases of China*, Sino-Dutch cooperation project report. Beijing, China: Institute of Water Resources and Hydropower Research.